

Eccentricity fluctuations in an integrated hybrid approach: Influence on elliptic flow

Hannah Petersen¹ and Marcus Bleicher²

¹*Department of Physics, Duke University, Durham, North Carolina 27708-0305, United States*

²*Frankfurt Institute for Advanced Studies, Johann Wolfgang Goethe-Universität,
Ruth-Moufang-Str. 1, D-60438 Frankfurt am Main, Germany*

The effects of initial state fluctuations on elliptic flow are investigated within a (3+1)d Boltzmann + hydrodynamics transport approach. The spatial eccentricity (ϵ_{RP} and ϵ_{part}) is calculated for initial conditions generated by a hadronic transport approach (UrQMD). Elliptic flow results as a function of impact parameter, beam energy and transverse momentum for two different equations of state and for averaged initial conditions or a full event-by-event setup are presented. These investigations allow the conclusion that in mid-central ($b = 5 - 9$ fm) heavy ion collisions the final elliptic flow is independent of the initial state fluctuations and the equation of state. Furthermore, it is demonstrated that most of the v_2 is build up during the hydrodynamic stage of the evolution. Therefore, the use of averaged initial profiles does not contribute to the uncertainties of the extraction of transport properties of hot and dense QCD matter based on viscous hydrodynamic calculations.

PACS numbers: 25.75.-q,24.10.Lx,24.10.Nz,25.75.Ld

I. INTRODUCTION

After the observations at the Relativistic Heavy Ion Collider (RHIC) that the elliptic flow measurements are consistent with ideal fluid dynamics predictions [1–3] the development of numerical solutions of viscous hydrodynamics equations is actively pursued [4–8]. The idea of those calculations is to quantify the deviations from local thermal equilibrium by comparisons to the available data for spectra and elliptic flow.

Solving the differential equations of any kind of fluid dynamics prescription implies the knowledge of the boundary conditions, i.e. the initial conditions and the freeze-out criterion. Therefore, it is essential to investigate in a systematic way how different initial profiles and freeze-out implementations influence the final observable results. This article focuses on this question concerning the initial conditions.

The realistic situation of the collision of two nuclei suffers from many different sources of initial state fluctuations [9]. The density profiles are not smooth, but there are peaks in the transverse and the longitudinal direction. There are impact parameter fluctuations within one specific centrality class leading to multiplicity fluctuations and differences in the initial geometry [10]. Furthermore, the nuclei do not necessarily collide in the event-plane given by the laboratory system, but might also have a rotated reaction plane. All these effects are averaged out, if assuming a smooth symmetric initial density profile as it is widely done by parametrising the initial conditions for hydrodynamic calculations within a Glauber or Color Glass Condensate (CGC) picture. To avoid potential misunderstandings, Monte-Carlo Glauber approaches (and CGC approaches) that produce fluctuating initial conditions are available and widely used, e.g. by experimental collaborations. However, usually these fluctuating initial conditions are not used as event-by-event initial conditions for the majority of hydrodynamic simulations. For alternative hydrodynamic approaches with

fluctuating initial conditions see e.g. [11, 12].

In this article an integrated Boltzmann+hydrodynamics transport approach is applied to the simulation of heavy ion reactions in the energy regime from $E_{\text{lab}} = 2 - 160A$ GeV. The initial conditions are generated by the Ultra-relativistic Quantum Molecular Dynamics (UrQMD) approach [13, 14] and the above mentioned event-by-event fluctuations are further propagated in the ideal hydrodynamic evolution employed for the hot and dense stage of the collision. On the other hand, calculations with averaged initial conditions are performed using the very same general setup. Comparing these calculations to the fluctuating setup the effect on the final observable elliptic flow is estimated.

II. INITIAL ECCENTRICITY

Let us start by looking at the initial state eccentricity as it is given by the UrQMD approach at the starting time $t_{\text{start}} = 2R/\sqrt{\gamma^2 - 1}$ of the hydrodynamic evolution. For the specific values of these times for Au+Au/Pb+Pb collisions at different beam energies see Table I. This is the earliest possible transition time at which local equilibrium might have been established after the two nuclei have passed through each other.

The eccentricity quantifies the spatial anisotropy of the initial state which is transformed via pressure gradients into a momentum space anisotropy in the transverse plane that can be quantified by the elliptic flow coefficient. The standard definition for the eccentricity is the reaction plane eccentricity

$$\epsilon_{\text{RP}} = \frac{\sigma_y^2 - \sigma_x^2}{\sigma_y^2 + \sigma_x^2}, \quad (1)$$

with $\sigma_x^2 = \langle x^2 \rangle - \langle x \rangle^2$ and $\sigma_y^2 = \langle y^2 \rangle - \langle y \rangle^2$. Especially

E_{lab} [GeV/nucleon]	t_{start} [fm]
2	12.417
6	7.169
11	5.295
40	2.830
160	1.415

TABLE I: Starting times of the hydrodynamic evolution for Au+Au/Pb+Pb collisions at different beam energies. The eccentricities displayed in Fig. 1 are also calculated at these times.

for smaller colliding systems the so called participant eccentricity is popular

$$\epsilon_{\text{part}} = \frac{\sqrt{(\sigma_y^2 - \sigma_x^2)^2 + 4\sigma_{xy}^2}}{\sigma_y^2 + \sigma_x^2}, \quad (2)$$

where an additional correlation term $\sigma_{xy} = \langle xy \rangle - \langle x \rangle \langle y \rangle$ is introduced. The participant eccentricity incorporates the fact that the participants themselves might be rotated with respect to the reaction plane. The averages $\langle \cdot \rangle$ indicate averages over all particles in one event and the mean eccentricity is obtained by averages over many UrQMD events. The standard deviation (shown as error bars in Fig.1) with respect to the event average is $\delta\epsilon = \langle \epsilon^2 \rangle - \langle \epsilon \rangle^2$.

Figs. 1 and 2 show the initial eccentricity in dependence of the beam energy for different centralities and

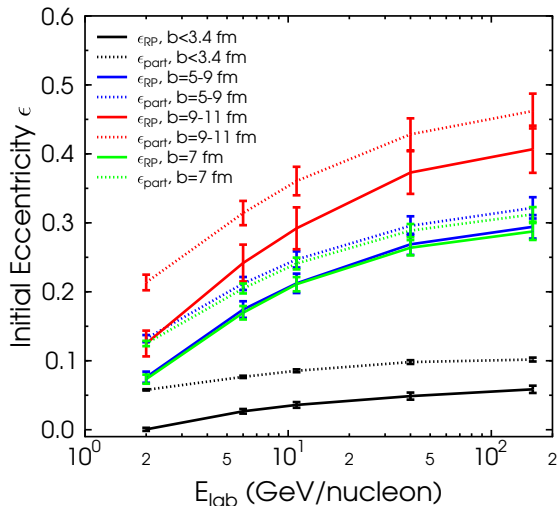


FIG. 1: (Color online) Initial eccentricity ϵ_{RP} (full lines) and ϵ_{part} (dotted lines) at time t_{start} for Au+Au/Pb+Pb collisions as a function of the beam energy. The results are shown for four different centrality selections, $b < 3.4$ fm, $b = 5 - 9$ fm, $b = 9 - 11$ fm and fixed impact parameter $b = 7$ fm. The standard deviation $\delta\epsilon$ is depicted as error bars to the mean value.

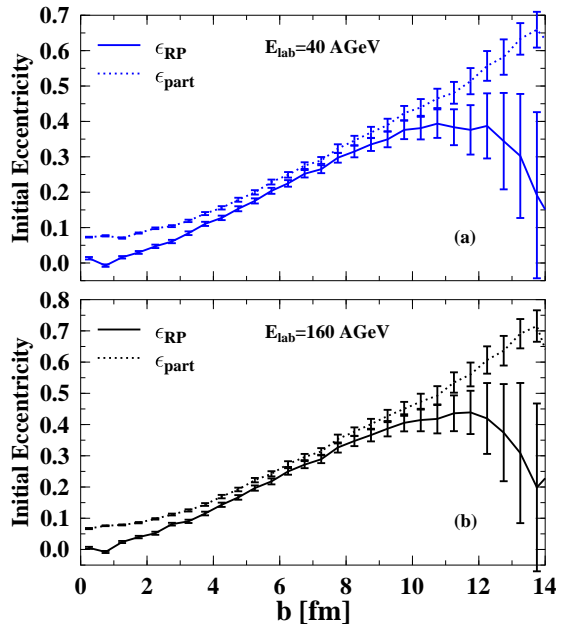


FIG. 2: (Color online) Initial eccentricity ϵ_{RP} (full lines) and ϵ_{part} (dotted lines) at time t_{start} for Pb+Pb collisions as a function of the impact parameter for $E_{\text{lab}} = 40A$ GeV (a) and $E_{\text{lab}} = 160A$ GeV (b). The standard deviation $\delta\epsilon$ is depicted as error bars to the mean value.

the impact parameter dependence for two different beam energies, respectively. The full lines depict the reaction plane eccentricity while the dotted lines refer to the participant eccentricity. In these calculations all particles which have suffered at least one interaction are included. This is consistent with the particles that are taken into account for the hydrodynamic evolution where the spectators are propagated separately in the cascade.

The initial eccentricity - mean value and standard deviation (as error bars) - as it is shown in Fig. 1 increases with the beam energy for both definitions. For simplicity the starting times are held constant with respect to the centrality variation. As expected the eccentricity is larger for more peripheral collisions. The participant eccentricity is always larger than the reaction plane eccentricity since it is calculated in the frame where the eccentricity is the largest possible one. Also the fluctuations of the eccentricity grow with increasing beam energy and with decreasing centrality of the collision. The fixed impact parameter calculation for $b = 7$ fm leads to very similar results as the $b = 5 - 9$ fm calculation for mid-central events. This hints to the fact, that centrality fluctuations have only a minor impact on the overall event-by-event fluctuations of the initial state.

Apart from the fact that the initial eccentricity at the highest SPS energy (see Fig. 2) is larger than at $E_{\text{lab}} =$

40A GeV the results for both energies are pretty similar. The reaction plane eccentricity is zero for small impact parameters while the participant eccentricity stays finite due to the rotation to the participant plane. Going to peripheral collisions the participant eccentricity increases almost linearly and the reaction plane eccentricity drops down again. The fluctuations grow much more for the reaction plane definition beyond an impact parameter of $b = 10$ fm. The most interesting observation from Fig. 2 is the small difference between ϵ_{RP} and ϵ_{part} and the very moderate fluctuations for mid-central collisions in the region of $b = 5 - 9$ fm. This behaviour is directly reflected in the centrality dependent elliptic flow results as it is shown in Section IV.

III. THE HYBRID APPROACH

To simulate the dynamic evolution of relativistic heavy ion reactions combined microscopic+macroscopic approaches have proven to be very successful in the description of various observables [15–25]. The approach that we are using here has recently been developed and is based on the UrQMD hadronic transport approach including a (3+1)-dimensional one fluid ideal hydrodynamic evolution [26, 27] for the hot and dense stage of the reaction while the early non-equilibrium stage and the final decoupling is treated in the hadronic cascade [28, 29] [44].

For the present investigation two in principal different setups are employed, but since they are constructed from the very same ingredients fair comparisons can be made. The first configuration is the integrated approach where the whole evolution from the incoming nuclei to final state particle distributions is calculated on an event-by-event-basis. The second possibility is to stop the UrQMD calculation at t_{start} and to average over many events at this time. These averaged initial conditions are then used to calculate the hydrodynamic evolution once and then the Cooper-Frye transition and the subsequent hadronic rescattering is averaged over many events again to obtain good statistics for the observables. In this second setup the spectators are not taken into account for the further evolution. To avoid spoiling the results by this difference in the setting we concentrate on observables at midrapidity.

In both setups the particles in the UrQMD initial state are mapped to energy, momentum and net baryon density distributions via three-dimensional Gaussian distributions that represent one particle each [30]. Two different equations of state are used to exemplify the differences due to this external input. One is a hadron gas equation of state (HG) with the same degrees of freedom as in the UrQMD approach [31]. The other one is a bag model equation of state (BM) including a strong first order phase transition to the quark gluon plasma with a large latent heat [27]. To see if fluctuations in the initial state affect the result differently for different expansion dynamics during the hydrodynamic evolution these two

extreme cases have been chosen.

The transition from the hydrodynamic evolution to the transport approach when the matter is diluted in the late stage is treated as a gradual transition on an approximated iso-eigntime hyper-surface (see [32] for details). The final rescatterings and resonance decays are taken into account in the hadronic cascade.

IV. ELLIPTIC FLOW RESULTS

The elliptic flow, the second coefficient of the Fourier expansion of the azimuthal distribution of the particles v_2 , quantifies the momentum anisotropy in the transverse plane [33–35]. It is a self-quenching effect, since the coordinate space asymmetry is transformed to a momentum space anisotropy until the system becomes isotropic. The elliptic flow is sensitive to the pressure gradients and therefore to the equation of state of the matter [36, 37]. It has also been shown that the elliptic flow is very sensitive to the shear viscosity that is present during the evolution.

In Fig. 3 the centrality dependence for the charged par-

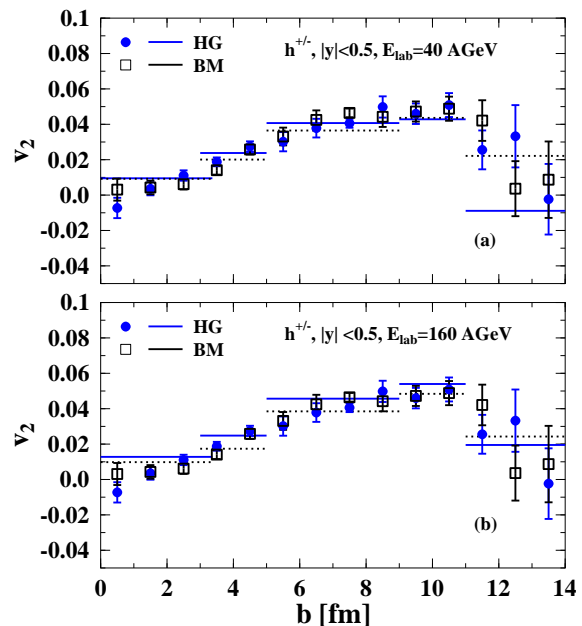


FIG. 3: (Color online) Centrality dependence of elliptic flow of charged particles at midrapidity ($|y| < 0.5$) for Pb+Pb collisions at $E_{lab} = 40A$ GeV (a) and $E_{lab} = 160A$ GeV (b). The horizontal lines indicate the results for averaged initial conditions using the hadron gas EoS (blue full line) and the bag model EoS (black dotted line) while the bag model EoS (black squares) and the hadron gas EoS (blue circles) depict the results for the event-by-event calculation.

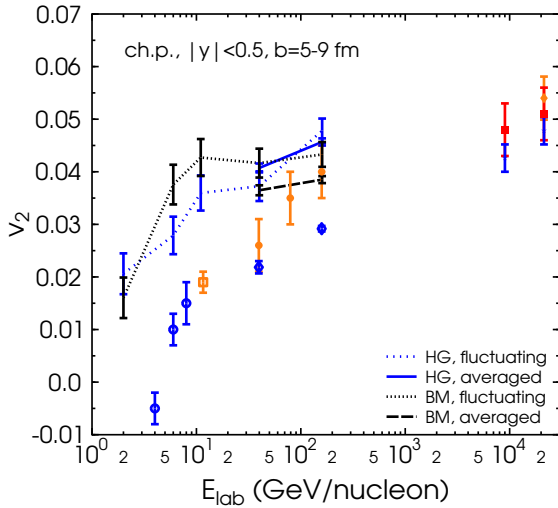


FIG. 4: (Color online) Excitation function of charged particle elliptic flow for mid-central Au+Au/Pb+Pb collisions in comparison to the experimental data (coloured symbols) [39, 40]. Results for the hadron gas EoS with averaged/fluctuating initial conditions are depicted as blue full/broken line while the calculations with the bag model EoS with averaged/fluctuating initial conditions are represented as black dashed/dotted line.

ticle elliptic flow is shown. The upper plot (a) presents results from the hybrid model for Pb+Pb collisions at $E_{\text{lab}} = 40A$ GeV while the lower plot (b) is for the highest SPS energy. The horizontal lines depict calculations for averaged initial conditions, while the symbols represent the full event-by-event-setup. Overall, the differences in the integrated elliptic flow between the two different calculations are small. Within the statistical error bars the averaged results are in line with the results including fluctuations for the corresponding centrality range. In accordance with the results for the impact parameter dependence of the initial eccentricity the fluctuations get larger for peripheral events. The highest elliptic flow values are reached for mid-central collisions ($b = 5 - 11$ fm). Therefore, we will refer to the impact parameter range from $b = 5 - 9$ fm for the following considerations.

Furthermore, calculations for the two different equations of state are shown. For the bag model EoS ('BM') the elliptic flow is expected to be smaller than for the hadron gas EoS ('HG') since the speed of sound during the expansion is smaller. This expectation is not fulfilled if one looks at the results [38]. The final elliptic flow results for different EoS are very similar and agree within the error bars. The softer expansion seems to be compensated by the longer lifetime of the system.

The calculation of the integrated elliptic flow at midrapidity in dependence of the beam energy (see Fig. 4) confirms the finding that the results do not depend on

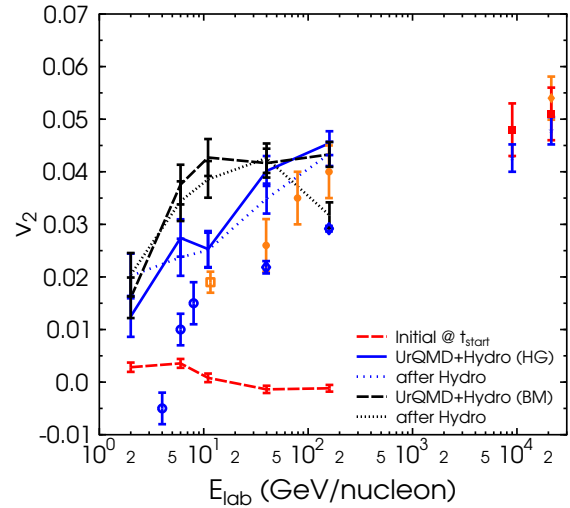


FIG. 5: (Color online) Excitation function of charged particle elliptic flow for mid-central Au+Au/Pb+Pb collisions in comparison to the experimental data (coloured symbols) [39, 40]. The initial state elliptic flow is shown as the red dashed line. The dotted lines refer to the end of the hydrodynamic evolution while the full lines represents full hybrid calculations for two different EoS.

the equation of state or on the initial condition setup. In the SPS range the results of the hybrid model calculations are in a reasonable agreement with the experimental data while at lower energies the generated elliptic flow is too high. Here, the inclusion of a mean field in the cascade part of the evolution helps to reproduce the data [41]. As it has been shown in [29] the elliptic flow at SPS energies might be affected by the transition from hydrodynamics to the hadronic transport model and leaves room for finite viscosities during the hydrodynamic expansion.

One might now conclude, that the elliptic flow has to be generated in the very early non-equilibrium stage and in the final state, if the results are not sensitive to the EoS during the hydrodynamic expansion and do not change if the overall setup is changed - event-by-event vs. averaged conditions. In Fig. 5 the contributions to the final elliptic flow value from the different stages of the evolution are shown. The elliptic flow in the initial state for the hydrodynamic expansion at t_{start} is compatible with zero at all beam energies. At early times, there is not enough transverse expansion to build up elliptic flow. The dotted lines show the elliptic flow directly after the Cooper-Frye transition at the end of the hydrodynamic expansion and at that time the final elliptic flow is already visible. The full lines correspond to the full calculation and indicates that only a small amount of elliptic flow is generated in the final and dilute stage of the collision. So, one is lead to the conclusion that the main part of the elliptic flow is indeed generated during the ideal hydrodynamic expan-

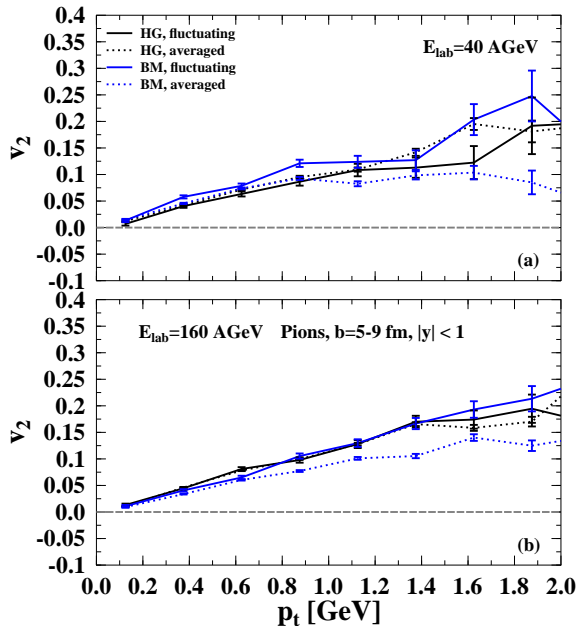


FIG. 6: (Color online) Transverse momentum dependence of elliptic flow of pions at midrapidity in mid-central Pb+Pb collisions at SPS energies ($E_{\text{lab}} = 40A$ GeV, (a) and $E_{\text{lab}} = 160A$ GeV, (b)). The full lines depict results for fluctuating initial conditions while the dotted lines refer to averaged initial conditions for two different EoS.

sion.

Let us now investigate the transverse momentum dependence of the elliptic flow results. The differential flow results might be more sensitive to the different setups. Fig. 6 shows the elliptic flow of pions at SPS energies for the two different equations of state. For the hadron gas equation of state the different setups lead to similar results again, while for the bag model the averaged initial conditions lead to reduced elliptic flow, especially at higher p_t . The Bag model equation of state seems to be more responding to the initial energy density fluctuations. If there are fluctuations, the transverse slices that freeze-out early and produce high transverse momentum particles have a longer time to expand because of the higher energy density spots whereas for the averaged conditions the whole system behaves more smoothly.

In Fig. 7 the transverse momentum dependence of the elliptic flow of protons at SPS energies is shown. The protons are interesting because they reflect the dynamics of the incoming nucleons and the finite net baryon density. For the protons the elliptic flow results are even less sensitive to either the EoS or the initial condition averaging than for the pions. At both energies all calculated v_2 curves are compatible with each other within error bars. The comparison to experimental data is postponed un-

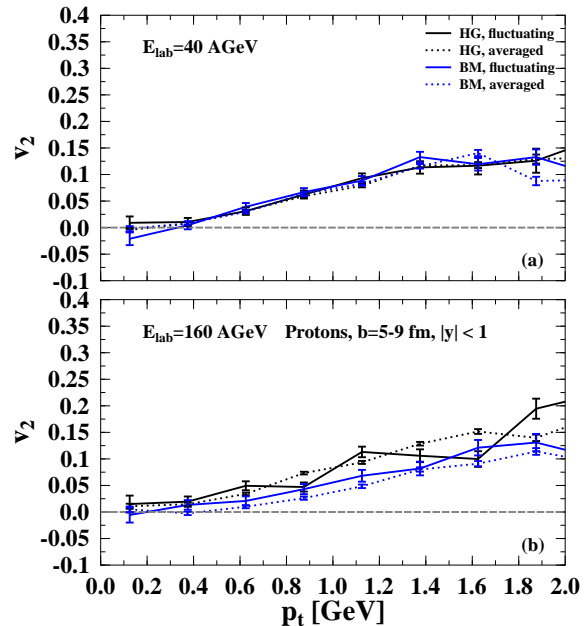


FIG. 7: (Color online) Transverse momentum dependence of elliptic flow of protons at midrapidity in mid-central Pb+Pb collisions at SPS energies ($E_{\text{lab}} = 40A$ GeV, (a) and $E_{\text{lab}} = 160A$ GeV, (b)). The full lines depict results for fluctuating initial conditions while the dotted lines refer to averaged initial conditions for two different EoS.

til more reliable results become available (for pions the comparison has been published in [38]).

V. SUMMARY AND CONCLUSIONS

The effect of initial state fluctuations on the finally measurable elliptic flow has been studied within a (3+1)d Boltzmann + hydrodynamics transport approach. The elliptic flow has been calculated as a function of the impact parameter, the beam energy and the transverse momentum for two different equations of state and for averaged initial conditions or a full event-by-event setup. These investigations allow for the conclusion that in mid-central ($b = 5 - 9$ fm) heavy ion collisions the final elliptic flow reaches its maximum and the fluctuations due to the initial state fluctuations are at a minimum. It has been confirmed that most of the v_2 is build up during the hydrodynamic stage of the evolution. The final integrated and differential elliptic flow for charged particles at SPS energies seems to be mostly sensitive to viscosity and not so much on the equation of state. Therefore, the use of averaged initial profiles does not contribute to the uncertainties for the extraction of transport properties of hot and dense QCD matter based on viscous hydrodynamic

calculations, while other ambiguities e.g. the contribution of the bulk viscosity [42] and different treatments of relaxation times for a multi-component system [43] remain under debate. Still the question if this statement is also valid at higher RHIC energies arises, since our approach in its present form can only be applied up to top SPS energies.

VI. ACKNOWLEDGEMENTS

We are grateful to the Center for the Scientific Computing (CSC) at Frankfurt for the computing resources.

The authors thank Dirk Rischke for providing the 1-fluid hydrodynamics code. This work was supported by GSI and BMBF. This work was supported by the Hessian LOEWE initiative through the Helmholtz International Center for FAIR (HIC for FAIR). H.P. acknowledges a Feodor Lynen fellowship of the Alexander von Humboldt foundation. This work was supported in part by U.S. department of Energy grant DE-FG02-05ER41367.

-
- [1] P. F. Kolb, P. Huovinen, U. W. Heinz and H. Heiselberg, Phys. Lett. B **500**, 232 (2001).
- [2] P. Huovinen, P. F. Kolb, U. W. Heinz, P. V. Ruuskanen and S. A. Voloshin, Phys. Lett. B **503**, 58 (2001).
- [3] L. P. Csernai, C. Anderlik, A. Keranen, V. K. Magas, J. Manninen and D. D. Strottman, Heavy Ion Phys. **17**, 271 (2003).
- [4] H. Song and U. W. Heinz, Phys. Lett. B **658**, 279 (2008).
- [5] H. Song and U. W. Heinz, Phys. Rev. C **77**, 064901 (2008).
- [6] M. Luzum and P. Romatschke, Phys. Rev. C **78**, 034915 (2008) [Erratum-ibid. C **79**, 039903 (2009)].
- [7] M. Luzum and P. Romatschke, Phys. Rev. Lett. **103**, 262302 (2009).
- [8] H. Song and U. W. Heinz, arXiv:0909.1549 [nucl-th].
- [9] T. Hirano and Y. Nara, Phys. Rev. C **79**, 064904 (2009).
- [10] W. Broniowski, M. Chojnacki and L. Obara, Phys. Rev. C **80**, 051902 (2009).
- [11] R. Andrade, F. Grassi, Y. Hama, T. Kodama and O. J. Socolowski, Phys. Rev. Lett. **97**, 202302 (2006).
- [12] K. Werner, T. Hirano, I. Karpenko, T. Pierog, S. Porteboeuf, M. Bleicher and S. Haussler, J. Phys. G **36**, 064030 (2009).
- [13] S. A. Bass *et al.*, Prog. Part. Nucl. Phys. **41**, 255 (1998) [Prog. Part. Nucl. Phys. **41**, 225 (1998)].
- [14] M. Bleicher *et al.*, J. Phys. G **25**, 1859 (1999).
- [15] C. Nonaka and S. A. Bass, Phys. Rev. C **75**, 014902 (2007).
- [16] A. Dumitru, S. A. Bass, M. Bleicher, H. Stoecker and W. Greiner, Phys. Lett. B **460**, 411 (1999).
- [17] S. A. Bass and A. Dumitru, Phys. Rev. C **61**, 064909 (2000).
- [18] D. Teaney, J. Lauret and E. V. Shuryak, Phys. Rev. Lett. **86**, 4783 (2001).
- [19] D. Teaney, J. Lauret and E. V. Shuryak, arXiv:nucl-th/0110037.
- [20] F. Grassi, Y. Hama, O. Socolowski and T. Kodama, J. Phys. G **31**, S1041 (2005).
- [21] R. Andrade, F. Grassi, Y. Hama, T. Kodama, O. J. Socolowski and B. Tavares, Eur. Phys. J. A **29**, 23 (2006).
- [22] T. Hirano, U. W. Heinz, D. Kharzeev, R. Lacey and Y. Nara, Phys. Lett. B **636**, 299 (2006).
- [23] T. Hirano, U. W. Heinz, D. Kharzeev, R. Lacey and Y. Nara, Phys. Rev. C **77**, 044909 (2008).
- [24] R. P. G. Andrade, F. Grassi, Y. Hama, T. Kodama and W. L. Qian, Phys. Rev. Lett. **101**, 112301 (2008).
- [25] R. P. G. Andrade, A. L. V. dos Reis, F. Grassi, Y. Hama, W. L. Qian, T. Kodama and J. Y. Ollitrault, Acta Phys. Polon. B **40**, 993 (2009).
- [26] D. H. Rischke, S. Bernard and J. A. Maruhn, Nucl. Phys. A **595**, 346 (1995).
- [27] D. H. Rischke, Y. Pursun and J. A. Maruhn, Nucl. Phys. A **595**, 383 (1995) [Erratum-ibid. A **596**, 717 (1996)].
- [28] H. Petersen, J. Steinheimer, G. Burau, M. Bleicher and H. Stoecker, Phys. Rev. C **78**, 044901 (2008).
- [29] H. Petersen and M. Bleicher, Phys. Rev. C **79**, 054904 (2009).
- [30] J. Steinheimer, M. Bleicher, H. Petersen, S. Schramm, H. Stoecker and D. Zschesche, Phys. Rev. C **77**, 034901 (2008).
- [31] D. Zschesche, S. Schramm, J. Schaffner-Bielich, H. Stoecker and W. Greiner, Phys. Lett. B **547**, 7 (2002).
- [32] Q. f. Li, J. Steinheimer, H. Petersen, M. Bleicher and H. Stoecker, Phys. Lett. B **674**, 111 (2009).
- [33] H. Sorge, Phys. Rev. Lett. **82**, 2048 (1999).
- [34] J. Y. Ollitrault, Phys. Rev. D **46**, 229 (1992).
- [35] M. Bleicher and H. Stoecker, Phys. Lett. B **526**, 309 (2002).
- [36] H. Stoecker and W. Greiner, Phys. Rept. **137**, 277 (1986).
- [37] S. A. Voloshin, A. M. Poskanzer and R. Snellings, arXiv:0809.2949 [nucl-ex].
- [38] H. Petersen, J. Steinheimer, G. Burau and M. Bleicher, Nucl. Phys. A **830**, 283C (2009).
- [39] C. Alt *et al.* [NA49 Collaboration], Phys. Rev. C **68**, 034903 (2003).
- [40] C. Pinkenburg *et al.* [E895 Collaboration], *Prepared for Centennial Celebration and Meeting of the American Physical Society (Combining Annual APS General Meeting and the Joint Meeting of the APS and the AAPT), Atlanta, Georgia, 20-26 Mar 1999*
P. Chung *et al.* [E895 Collaboration], Phys. Rev. C **66**, 021901 (2002)
K. Filimonov *et al.* [CERES/NA45 Collaboration], arXiv:nucl-ex/0109017.
J. Slivova [CERES/NA45 Collaboration], Nucl. Phys. A **715**, 615 (2003)
S.I.Esumi, J. Slivova, J. Milosevic for CERES Collaboration Physics,” SFIN, year XV, Series A: Conferences, No. A2(2002)
S. Esumi [PHENIX Collaboration], Nucl. Phys. A **715**,

- 599 (2003)
S. Manly *et al.* [PHOBOS Collaboration], Nucl. Phys. A **715**, 611 (2003)
R. L. Ray [STAR Collaboration], Nucl. Phys. A **715**, 45 (2003)
- [41] H. Petersen, Q. Li, X. Zhu and M. Bleicher, Phys. Rev. C **74**, 064908 (2006).
- [42] G. S. Denicol, T. Kodama, T. Koide and Ph. Mota, Phys. Rev. C **80**, 064901 (2009).
- [43] A. Monnai and T. Hirano, arXiv:1003.3087 [nucl-th].
- [44] The code is available as UrQMD-3.3 at <http://urqmd.org>